Effect of Cytarabine on the NMR Structure of a Model Okazaki Fragment from the SV40 Genome†

William H. Gmeiner,*,‡ David Konerding,§ and Thomas L. James||

Eppley Institute and Department of Pharmaceutical Sciences, University of Nebraska Medical Center, Omaha, Nebraska 68198-6805, Graduate Group in Biophysics and Department of Pharmaceutical Chemistry, University of California, San Francisco, California 94143

Received July 15, 1998; Revised Manuscript Received November 11, 1998

ABSTRACT: Okazaki fragments occur as intermediates during lagging strand DNA replication. Alterations in Okazaki fragment structure may contribute to the anticancer activities of nucleoside analogues such as cytarabine, a potent anti-leukemic agent that inhibits lagging strand replication. We have determined the solution structures for two model Okazaki fragments, [OKA] and [ARAC]. These sequences are derived from a frequent initiation site for primase during replication of the SV-40 viral genome. The sequence of [ARAC] differs from [OKA] only by substitution of cytarabine for one deoxycytidine. The structure of each model Okazaki fragment was elucidated using NMR spectroscopy and restrained molecular dynamics simulations. The solution structures of [OKA] and [ARAC] each consist of two distinct domains: a DNA duplex region (DDR) and an RNA−DNA hybrid duplex region (HDR). The DDR of [OKA] adopts geometry similar to B-form except for variations in helical parameters, especially twist and roll, which occur in the purine tract, increasing base overlap among the five consecutive purines. The helical axes for the DDR and HDR of [OKA] are bent 22° relative to one another. Although the local structures for the DDR and HDR of [ARAC] are similar to those in [OKA] (root-mean-square deviation (rmsd) ∼0.8, 1.7 Å), the bending at the junction is different (41° for [ARAC] vs 22° for [OKA]). Increased helical bending of cytarabine-substituted Okazaki fragments may contribute to the propensity of cytarabine to inhibit elongation of the lagging strand during DNA replication, and in effecting anticancer activity.

Biochemical studies from a number of organisms indicate that similar sequences, and hence structural motifs, occur at the origin sites for all autonomously replicating sequences (ARS[1] elements) that are required for initiation of DNA replication (*1*−*4*). Once replication is initiated near the ARS, the two parental strands of the DNA duplex are unwound by helicase activities, and continuous DNA replication occurs at the leading strand of the replication fork by addition of nucleotides in the 5′ → 3′ direction to form one new daughter strand (*5*). The second daughter strand results from replication of the lagging DNA strand at the replication fork. Lagging strand replication occurs discontinuously, and requires synthesis of an RNA primer that is extended by addition of deoxynucleotides, also in the 5′ → 3′ direction. Completion of DNA replication requires excision of the RNA primer by RNAse H1 and FEN1, and ligation of the DNA chains (*6*). Okazaki fragments occur as intermediates during replication of the lagging strand, and contain the RNA primer, and the nascently synthesized DNA associated with the lagging DNA strand through complementary base pairing (*7*). Okazaki fragments are thus RNA−DNA hybrid duplexes covalently linked to duplex DNA. The relative infrequency with which nature utilizes the hybrid duplex motif characteristic of Okazaki fragments makes information concerning Okazaki fragment structures valuable in understanding the structural basis underlying semiconservative replication (*8*, *9*).

The rate of replication for nuclear DNA is often elevated in malignant cells, particularly in aggressive tumors, relative to surrounding healthy tissues (*10*). Interference in DNA replication of malignant cells inhibits tumor expansion, and may reduce tumor mass if unsuccessful replication induces tumor cell death (*11*). A substantial fraction of effective anticancer drugs target nuclear DNA and interfere in replication (*12*). Several of these drugs bind to duplex DNA, either covalently or noncovalently (refs *13*−*15*; reviewed in ref *16*). Nucleoside analogues such as cytarabine (1-β-D-arabinofuranosylcytosine; Figure 1), in contrast, are sufficiently similar to native nucleosides in structure that they are taken

† This work was supported in part by NIH CA-60612 (W.H.G.), NIH CA-36727 (W.H.G.), NIH GM-39247 (T.L.J.), and the Nebraska Department of Health (W.H.G.).

* To whom correspondence should be addressed. (402) 559-4257. Fax: (402) 559-4651. E-mail: bgmeiner@unmc.edu.

‡ University of Nebraska Medical Center.

§ Graduate Group in Biophysics, University of California.

|| Department of Pharmaceutical Chemistry, University of California.

[1] Abbreviations: [ARAC], model Okazaki fragment containing a single cytarabine substitution; ARS, autonomously replicating sequences; CORMA, complete relaxation matrix analysis; CPMG, Carr Purcell Meiboom Gill experiment; Cytarabine, 1-β-D-arabino-furanosylcytosine; DDR, DNA duplex region of [OKA]; ECOSY, exclusive correlated spectroscopy; FID, free induction decay; HDR, hybrid duplex region of [OKA]; JR, junction region of [OKA]; MARDIGRAS, matrix analysis of relaxation for discerning the geometry of an aqueous structure (algorithm); [OKA], model Okazaki fragment; PFG, pulsed field gradient; HPLC, high-performance liquid chromotography; rMD, restrained molecular dynamics; rmsd, (atomic) root-mean-square deviation; SV-40, Simian virus 40; TOCSY, total correlation spectroscopy.

10.1021/bi981702s CCC: $18.00
Published on Web 01/05/1999

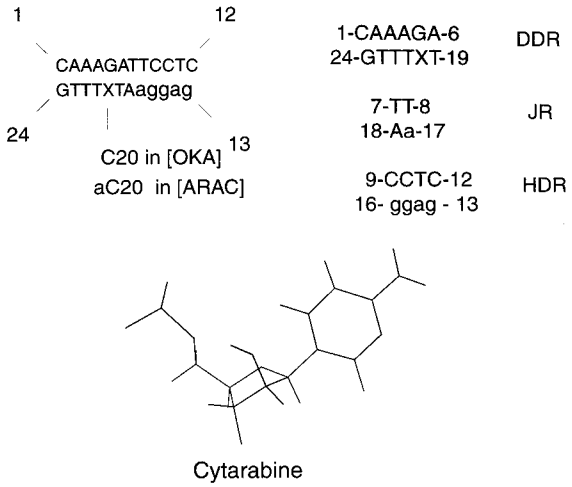

FIGURE 1: The sequences for the [OKA] and [ARAC] model Okazaki fragment sequences are shown at the left, and the sequences for the DNA duplex region (DDR), junction region (JR), and hybrid duplex region (HDR) of [OKA] and [ARAC] are shown at the right. Deoxyribonucleosides are indicated in uppercase and ribonucleosides in lower case in the figure and throughout the text. The site of cytarabine substitution in [ARAC] and in the DDR of [ARAC] is designated with an X. First and last residues for each strand are numbered. The sequence is derived from one of the principal initiation sites of primase during lagging strand replication of the SV-40 viral genome.

up by nucleoside transport proteins and metabolized to 5′-*O*-triphosphate forms that are incorporated directly into the nuclear DNA (*17*, *18*). Once incorporated into the nascent DNA during the course of replication, nucleoside analogues may inhibit successful completion of replication by altering the structure, stability, or protein binding characteristics of DNA (*19*). In the present manuscript, we investigate the effect of cytarabine substitution for one deoxycytidine on the solution structure of a model Okazaki fragment derived from the SV-40 viral genome (*20*). Cytarabine is an analogue of deoxycytidine that is effective in the treatment of leukemia (ref *21*; Figure 1). Evidence that cytarabine may exert its anticancer effect by altering Okazaki fragment structure comes from analysis of nascent DNA from cells exposed to cytarabine. Cytarabine inhibits DNA elongation, with inhibition occurring predominantly at the lagging strand of the replication fork, and only after considerable extension (~100 nucleotides) of the nascent DNA following the site of substitution (*22*). The propensity of cytarabine to interfere with extension of the lagging strand a considerable distance from the site of substitution suggests that it affects the local structure, and/or stability, of newly replicated DNA, inhibiting extension of the nascent DNA at a point distal from the site of substitution.

At present, a limited number of structural investigations of Okazaki fragments have been reported, and only a few high-resolution structures are available (*23*−*30*). Rich and co-workers reported the X-ray structure of an Okazaki fragment at 2 Å resolution (*29*). The structure of this Okazaki fragment in the crystal was A-form. Although the structure was distorted at the RNA−DNA junction, no transition from A- to B-form was observed. In contrast, the NMR solution structure for the same Okazaki fragment sequence suggested a global duplex structure that differs from either A- or B-form, with structural discontinuities at the RNA−DNA junction of the hybrid strand (*30*). In the present manuscript, we present the NMR solution structures for a model Okazaki fragment derived from the SV-40 viral genome, with and without cytarabine substitution (*19*). These structures consist of three distinct regions, each of which has a characteristic nucleoside composition and adopts a distinct morphology.

Although the overall conformation of the DNA duplex region (DDR; see Figure 1) of [OKA] is similar to the B-form, substantial deviations in roll and twist are observed inside the purine tract that maximize base stacking. The site of cytarabine substitution occurs in the DDR of [ARAC] (Figure 1), although the nomenclature is retained to permit comparison between [OKA] and [ARAC]. Cytarabine-induced structural changes in the DDR of [ARAC] relative to [OKA] are subtle. Twist and roll values in the DDR of [ARAC] are more similar to canonical B-form DNA than for [OKA], and the sugar pucker for the arabinosyl nucleoside is C2′-endo. The geometry of the DDR for [ARAC] results in less efficient stacking among adjacent purines than was observed for [OKA]. This less efficient stacking may provide the basis for the reduced stability of [ARAC] relative to [OKA] (*19*). The hybrid duplex regions (HDR) of [OKA] and [ARAC] are similar. The HDR in each duplex adopts H-form geometry, with the ribonucleosides adopting A-form geometry and the deoxyribonucleosides adopting either H-form or B-form geometry, depending on proximity to the terminus. The junction regions (JR) of [OKA] and [ARAC] each have base stacking properties similar to B-form, although torsion angles varied considerably from canonical B-form values. The most significant structural difference between [ARAC] and [OKA] is a substantial increase in the bend of the helical axis from 22° to 41°. This increased bending occurs at the site of cytarabine substitution, and may contribute to the inhibition of DNA extension during replication that may explain the anticancer activity of cytarabine.

MATERIALS AND METHODS

Synthesis of Model Okazaki Fragments. The sequences for the [OKA] and [ARAC] model Okazaki fragments are shown in Figure 1. The DNA strand of [ARAC] is identical to that in [OKA] and was prepared using standard automated methods with a Perkin-Elmer/Applied Biosystems Division 394 DNA synthesizer. The hybrid strands are composed of deoxyribo- and ribonucleosides for [OKA], and deoxyribo-, ribo-, and arabinonucleosides for [ARAC]. The hybrid strands were prepared as previously described (*19*). For the incorporation of cytarabine, 1-β-D-arabino-furanosylcytosine (cytarabine) was purchased from Sigma and was converted to a suitably protected 3′-*O*-phosphoramidite using methods similar to those previously described (*31*). Briefly, the approach involves bis-protection of the 3′-OH and 5′-OH groups with a disiloxane reagent followed by acetylation at the 2′-OH and N4 amino group. The 3′-OH and 5′-OH were then deprotected with tetrabutlyammonium fluoride. Tritylation with the bulky reagent 4,4′-dimethoxytrityl chloride occurred selectively at the 5′-OH and was followed by phosphoramidation of the 3′-OH. The resulting 5′-*O*-dimethoxytrityl-3′-*O*-phosphoramidite was purified by column chromatography, and incorporated in place of one deoxycytidine (aC20, see Figure 1) during the chemical synthesis of the hybrid strand of [ARAC]. Synthesis of each strand was performed using the RNA 10 μmol scale synthesis

cycle with Tr-Off/manual ending. The CPG support was removed from the synthesis column and transferred to a glass screw-capped tube, and anhydrous methanol (3−4 mL) was added. The solution was saturated with ammonia, sealed, and heated overnight at 50 °C. The methanol solution was carefully removed from the support and evaporated to dryness. The residue was redissolved in neat triethylamine trihydrofluoride (750 μL) and left to stir overnight at room temperature. Water (2 mL) was added to dissolve the white suspension, and the solution was evaporated to a thick oil (∼100 μL). The oil was redissolved in water, and aliquots (∼250 A_{260} units) were purified by anion-exchange HPLC using a Waters DEAE−5PW (22.5 mm × 150 mm) column using an aqueous sodium perchlorate gradient. Fractions containing product were pooled, concentrated by evaporation, and desalted using Sephadex G-25.

NMR Spectroscopy. All NMR experiments were performed using a Varian UNITY 500 NMR spectrometer equipped with a 3 mm ^{1}H{^{13}C, ^{31}P} PFG probe. Samples for NMR analysis were prepared by mixing equimolar amounts of the two strands. Each sample contained about 30 absorbance units of one duplex in 220 μL of 2 mM sodium cacodylate (pH 7.3), 100 mM NaCl, and 0.2 mM disodium EDTA. ^{1}H spectra were referenced to HDO at 4.76 ppm at 26 °C. NOESY spectra in D_2O were acquired for mixing times of 100, 150, and 200 ms using the standard three-pulse sequence with States' method of phase cycling (*32*). Four hundred free induction decays (FID), 16 scans each, with alternating block acquisition, were collected in the t_1 dimension. 2048 data points over a spectral width of 5000 Hz were collected in the t_2 dimension with the carrier frequency set at the ^{1}HDO resonance. A relaxation delay of 10 s was included between scans to allow adequate relaxation for cross-peak quantitation. TOCSY spectra were acquired with 60 and 100 ms mix times using parameters similar to those described for NOESY spectra, except the relaxation delay was shortened to 3 s. ECOSY spectra were collected using 32 scans per increment with a 3 s relaxation delay and 4096 points in t_2 (*33*). All data were initially processed using VNMR v. 5.3B from Varian and then imported into SPARKY (UCSF) for analysis. The spectra were apodized in both dimensions using shifted Gaussian filter functions. After zero-filling in the t_1 dimension, the final matrices were 2048 × 2048 points, except for ECOSY spectra that were 4096 × 2048 points. T1 and T2 values were obtained from inversion−recovery and CPMG experiments, respectively, and were fit to single-exponential functions using VNMR v. 5.3B.

Experimental Constraints. Constraints on interproton distances and torsion angles were determined from NOESY and ECOSY data sets, respectively. Interproton distances were calculated from NOESY cross-peak intensities using MARDIGRAS (*34*). Volume integrals for [OKA] were evaluated for 382 and 380 cross-peaks from NOESY experiments acquired with 100 and 200 ms mix times, respectively. Volume integrals for [ARAC] were evaluated for 398 and 343 cross-peaks from NOESY experiments acquired with 150 and 200 ms mix times, respectively. Instrumental instability prevented evaluation of the 150 ms mix time NOESY for [OKA] and the 100 ms mix time NOESY of [ARAC]. The robustness of MARDIGRAS permitted accurate estimation of interproton distance bounds from two NOESY datasets for each duplex. NOESY intensities evaluated for cross-peaks on both sides of the diagonal were averaged. A complete relaxation matrix was created for both [OKA] and [ARAC] using intensities evaluated experimentally for 240 interproton interactions, and estimated intensities from the geometry of the starting structure for those interproton interactions that could not be evaluated from the experimental data. The diagonal and off-diagonal terms were compared iteratively until the sum of the residual errors was minimized. MARDIGRAS calculations for [OKA] and [ARAC] were carried out with two experimental data sets (100, 200 ms for [OKA]; 150, 200 ms for [ARAC]), two geometries for the initial structure (A-form and B-form double helices), and four values for the isotropic correlation time (τ_c = 1.1, 1.4, 1.7, and 4.8 ns). A value of 1.4 ns for τ_c was calculated from the T1 and T2 relaxation data according to previously published procedures, while a value of 4.8 ns for τ_c was reported for an Okazaki fragment under similar conditions (*30*, *35*). Estimates of interproton distances associated with NOE cross-peak intensities resulting from each of the sixteen MARDIGRAS calculations for each duplex were averaged. The average distance and standard deviation were then used to set the flat portion of the potential well for each distance constraint.

Torsion angles for the ribose and deoxyribose sugars were determined from the estimation of $^3J_{HH}$ from ECOSY spectra (*36*, *37*). The pseudorotational angle *P* for deoxyribose sugars was calculated from $^3J_{H1'-H2'}$, $^3J_{H1'-H2''}$, and $^3J_{H3'-H4'}$ using a modified Karplus relationship (*36*, *38*). The sugar torsion angles $\upsilon_0-\upsilon_4$ were determined from *P* using the following equation (*39*):

$$\upsilon_j = T_m \cos[P + 144(j - 2)] \quad (1)$$

The value of T_m was estimated as 38.5° (*36*). Values of the torsion angle χ_1 were determined from intraresidue H8/H6−H2′ and H8/H6−H2″ distances derived from the MARDIGRAS calculations, and from *P* values consistent with the ECOSY data.

Restrained Molecular Dynamics. Initial structures for [OKA] and [ARAC] were constructed with A-form and B-form double helical geometry using SYBYL (Tripos, Inc.). The arabinosyl sugar of [ARAC] was constructed by adding an oxygen of the appropriate stereochemistry to C2′ of aC20 (Figure 1). The retention of appropriate stereochemistry for the C2′ hydroxyl of aC20 was verified at all subsequent stages of refinement. Coordinate and topology files were created for each geometry using the LEAP module of AMBER 4.1 (UCSF). Large, hexahydrated sodium ions with a 5 Å radius were added to mimic counterion effects. These counterions were placed along the phosphate bisection, 6 Å away from the phosphorus, and were free to move during energy minimization and molecular dynamics procedures (*40*). The starting structures were energy-minimized in vacuo using a combination of steepest descents and conjugate gradient methods with the SANDER module of AMBER 4.1.

Restrained molecular dynamics (rMD) simulations were carried out in vacuo, also using the SANDER module of AMBER 4.1. Distance and angular constraints were included in the force field as pseudoenergy terms, which had the form of a flat well with parabolic sides extending 0.5 Å or 5° beyond these margins, and linearly increasing beyond the parabolic region (*41*). The MARDIGRAS bounds determined

the width of the flat portion of the potential well (*42*). Pseudorotation angles for the sugar pucker were estimated to be within 10° of the time-averaged value, and this range, in conjunction with eq 1, was used to establish the flat portion of the potential well for the individual dihedral angles. The backbone dihedral angles were constrained in a broad allowed region of the torsional angle space to preserve the right-handed character of the double helix that was evident from the NOESY spectra (*43*). Additional distance and angular constraints were added between the bases to maintain Watson−Crick geometry during rMD simulations. These Watson−Crick hydrogen bond constraints were consistent with the direct observation of signals from imino and amino ^{1}H resonances (*19*).

Initial structures (energy-minimized A- and B-form geometry) were subjected to a 30 ps rMD simulation with the constraints included as pseudoenergy terms. Initial velocities were taken from a Maxwellian distribution at 0.4 K. The system was then heated gradually from 100 to 450 K during the first 5000 (fs) steps. The system was maintained at 450 K for 10 000 steps and then gradually decreased over 5000 steps to a final value of 300 K. The constraints were modulated by multiplying the force constant with a scaling factor as previously described (*44*). The coordinates for the last 5 ps of the dynamics trajectory were averaged, and this procedure was repeated for three seed velocities for both the initial A- and B-form structures. The coordinates resulting from each of the three trajectories for both initial A- and B-form geometries were averaged and energy-minimized, resulting in final A- and B-form structures. The coordinates for these two structures were then averaged and energy-minimized, and the resulting hybrid structure was subjected to 20 ps of rMD at 300 K (*45*). The solution structures of [OKA] and [ARAC] were obtained from identical, but independent, protocols by averaging the coordinates for the final 5 ps of the final rMD trajectory, followed by 1000 steps of restrained energy minimization. Means and standard deviations for torsional angles and helical parameters for these structures were determined from analysis of the final, 20 ps rMD trajectory using the programs CURVES (*46*) and DIALS and WINDOWS (*47*).

Intermediate and final structures were analyzed for compliance with the experimental constraints using CORMA (UCSF; ref *48*). A summary of sixth root index compliance and rmsd values between intermediate and final structures for [OKA] and [ARAC] is included in the Supplementary Information.

RESULTS

Resonance Assignments. The residue numbering for the [OKA] model Okazaki fragment is given in Figure 1. The ^{1}H resonance assignments for the 19 deoxyribose sugars of [OKA] were made on the basis of scalar connectivities using TOCSY and ECOSY spectra. All of the deoxyribose sugars displayed H1′−H2′/H2″, H3′−H2′/H2″, H3′−H1′, H3′−H4′, and H4′−H5′/H5″ cross-peaks in the TOCSY spectrum (60 ms mix) permitting complete resonance assignment (Tables 1 and 2; TOCSY spectra are included in the Supporting Information). Stereochemical assignments for H2′/2″ were made on the basis of the relative intensities of the H1′−H2′/H2″ cross-peaks for NOESY spectra acquired with 100 ms mix time. H2″ resonated downfield of H2′ for all deoxyribose sugars except for G5. Sequential connectivity between the deoxyribose spin systems was established by the observation of (*n*)H8/H6-(*n*)H1′ and (*n*)H8/H6-(*n-1*)H1′ and/or (*n*)H8/H6-(*n*)H2′/H2″ and (*n*)H8/H6-(*n-1*)H2′/H2″ cross-peaks in the NOESY spectrum (*49*). The ribose spin systems were assigned on the basis of (*n*)H1′-(*n*)H2′ and (*n*)-H8/H6-(*n-1*)H2′ cross-peaks in NOESY spectra and H3′−H4′ cross-peaks in TOCSY, ECOSY, and DQCOSY spectra (Table 2; Supplementary Information). Sequential connectivities for both types of nucleotides were also apparent from (*n-1*)H8/H6-(*n*)H5/M cross-peaks in NOESY spectra. With the exception of the arabinosyl nucleoside, identical procedures were used to assign the resonances of [ARAC] as were used for [OKA]. The arabinosyl spin system was assigned on the basis of (*n*)H1′-(*n*)H2″ in NOESY, TOCSY, and ECOSY spectra, and a similar pattern of sequential NOEs as for the deoxyribonucleotides. Differences in chemical shift between [OKA] and [ARAC] are shown in Table 3.

Table 1: ^{1}H Resonance Assignments for the DNA Strand of [OKA]

	H8/H6	H5/H2/M	H1′	H2′	H2″	H3′	H4′
C1	7.64	5.97	5.62	1.72	2.27	4.66	4.03
A2	8.28	7.41	5.72	2.75	2.82	5.00	4.32
A3	8.10	7.24	5.85	2.62	2.82	5.04	4.41
A4	7.95	7.44	5.94	2.55	2.80	5.02	4.41
G5	7.93		6.16	2.63	2.37	4.71	4.17
A6	7.90	7.83	6.21	2.65	2.85	4.82	4.42
T7	7.21	1.36	5.85	2.10	2.56	4.74	4.21
T8	7.56	1.55	6.07	2.36	2.59	4.85	4.25
C9	7.58	5.54	5.94	2.34	2.53	4.70	4.24
C10	7.49	5.40	5.83	2.26	2.59	4.63	4.22
T11	7.63	1.51	6.10	2.30	2.60	4.85	4.24
C12	7.61	5.62	6.27	2.17	2.25	4.53	4.06

Table 2: ^{1}H Resonance Assignments for the RNA−DNA Strand of [OKA][a]

	H8/H6	H5/H2/M	H1′	H2′	H2″	H3′	H4′
g13	8.01		5.68	4.84		4.64	4.62
a14	8.08	7.77	6.06	4.81		4.56	4.57
g15	7.22		5.62	4.62		4.43	4.48
g16	7.17		5.68	4.64		4.48	4.39
a17	7.68	7.88	5.85	4.61		4.48	4.56
A18	7.76	7.33	6.09	2.44	2.78	4.65	4.35
T19	7.46	1.11	6.08	2.23	2.58	4.85	4.21
C20	7.61	5.54	6.08	2.19	2.59	4.84	4.26
T21	7.49	1.64	6.10	2.21	2.59	4.91	4.18
T22	7.51	1.72	6.12	2.18	2.59	4.91	4.21
T23	7.35	1.78	5.92	2.00	2.42	4.89	4.12
G24	7.91		5.61	2.53	2.65	4.92	4.36

[a] RNA nucleotides designated lowercase.

Structures of [OKA] and [ARAC]. Okazaki fragments are characterized by a hybrid RNA−DNA duplex covalently attached to a DNA duplex. Since long-range contacts are generally absent in nucleic acid fragments having size amenable to NMR spectroscopic analysis, the solution structures of [OKA] and [ARAC] may be considered in terms of the local structures adopted by the DNA duplex region (DDR), the RNA−DNA hybrid duplex region (HDR), and the base pairs at the junction of these two distinct duplex regions (JR) (Figures 2 and 3). The structure of [OKA] may thus be considered as being composed of the local structures adopted by each of these three regions. The sequence of [ARAC] is identical to [OKA], except cytarabine is substituted for one deoxycytidine (C20 → aC20; see Figure 1).

Table 3: Chemical Shift Differences in [ARAC] Compared to [OKA][a]

	H8/H6	H5/H2/M	H1′	H2′	H2″
A3	+0.03	+0.03	+0.02	+0.01	+0.01
A4	+0.06	+0.03	+0.07	+0.07	+0.02
G5	+0.03		+0.02	+0.01	+0.01
A6	−0.05	+0.05	+0.02	+0.00	−0.01
T7	+0.05	−0.02	+0.02	+0.03	+0.03
A18	+0.03	+0.03	+0.02	+0.01	+0.01
T19	+0.00	+0.01	+0.15	−0.06	+0.15
aC20	−0.16	−0.14	−0.19		+1.88
T21	−0.16	−0.08	−0.11	−0.06	+0.01
T22	+0.00	+0.00	+0.03	+0.01	+0.00

[a] Positive numbers denote that the resonance is further downfield in [ARAC] than in [OKA].

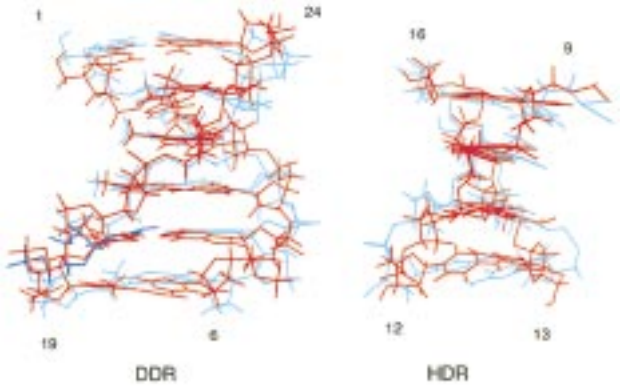

FIGURE 2: Superimposition of the DDR (left) and HDR (right) for [OKA] (red) and [ARAC] blue (aC20 in dark blue). Although the DDR and HDR regions superimpose reasonably well (rmsd ~0.8, 1.7 Å), the entire structures superimpose poorly (~4.2 Å), resulting from a distinctly greater bend in the helical axis for [ARAC] relative to [OKA] (41° vs 22°; see Figure 4).

As will be described in greater detail below, the DDR of both [OKA] and [ARAC] adopts a modified B-form geometry. The HDR of both model Okazaki fragments adopts residue-specific geometry with the ribonucleosides (g13-g16) adopting A-form geometry while the complementary deoxyribonucleosides (C9−C12) adopt time-averaged sugar puckers intermediate between those characteristic of A- and B-form helices (except for the two nucleosides nearest the 3′-terminus of the DNA strand that adopt C2′-endo sugar puckers). The two nucleosides in the DNA strand (T7 and T8) at the junction region (JR) that link the DDR and HDR also adopt time-averaged sugar puckers intermediate between A- and B-form helical geometry in both model Okazaki fragments, as does the DNA residue of the hybrid strand in the JR (A18). The ribonucleoside of the RNA−DNA base pair of the JR adopts A-form geometry (a17). Overall, the solution structure of [OKA] more closely resembles B-form rather than A-form DNA, although substantial deviations from this ideal geometry occur in all regions of the structure (*50*). The most obvious structural difference between [OKA] and [ARAC] is an increase in the helical bend for [ARAC] (Figure 4).

DDR Structures. The DNA duplex region (DDR) of [OKA] consists of deoxyribonucleosides C1-A6 and T19-G24 (Figure 1). The DDR of [ARAC] comprises the same residues, but includes aC20, the site of cytarabine substitution (Figure 1). Inspection of the DDR for the solution structure of [OKA] (Figure 2) reveals that the DDR adopts B-form

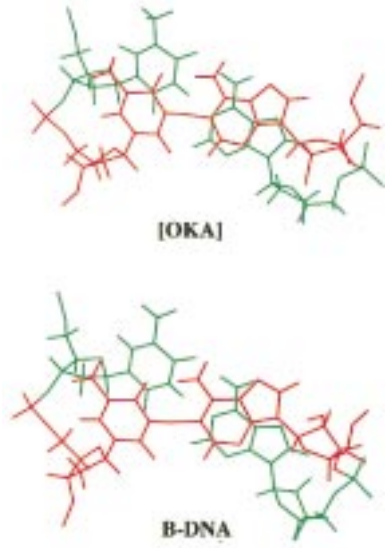

FIGURE 3: View along the dyad axis showing stacking between nucleosides in the JR of the refined structure of [OKA] (top) and the energy-minimized B-form geometry (bottom). For each duplex the DNA−DNA base pair (T7-A18) is shown in aqua and the RNA−DNA base pair (T8-a17) is shown in red. Examination of backbone torsion parameters (Supplementary Information) shows considerable deviation from B-form values for most parameters in this region of [OKA]. This view along the dyad axis shows that purine-purine stacking in the JR is enhanced slightly for [OKA] but is similar to that for B-form helices. Base stacking and sugar puckers for [ARAC] in the JR resemble [OKA].

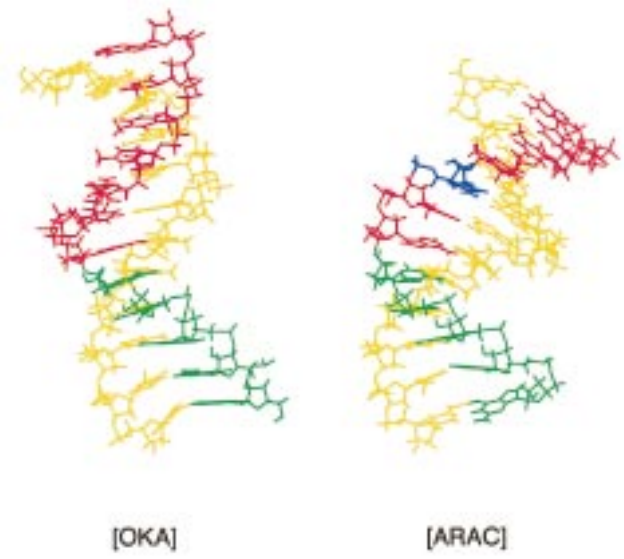

FIGURE 4: Representation of the van der Waals surface for the time-averaged structures of the [OKA] (left) and [ARAC] (right) model Okazaki fragments. Sequences for both duplexes are shown in Figure 1. Coordinates for [OKA] and [ARAC] were matched on the residues that comprise the HDR (see Figure 2). The DNA strand for each duplex is shown in yellow, while the ribonucleosides of the hybrid strand are in green and the deoxyribonucleosides of the hybrid strand are in red. Cytarabine is shown in blue. Although both model Okazaki fragments show a bend between the DDR and HDR, [ARAC] shows a pronounced increase in helical bend, relative to [OKA], at the site of cytarabine substitution (41° vs 22°).

geometry, and analysis of the helical parameters and torsion angles for the DDR is generally consistent with this interpretation (Supplementary Information). The sugar puckers for all of the deoxyribonucleosides in the DDR of [OKA] are C2′-endo, except for T22 which adopts a C1′-exo sugar

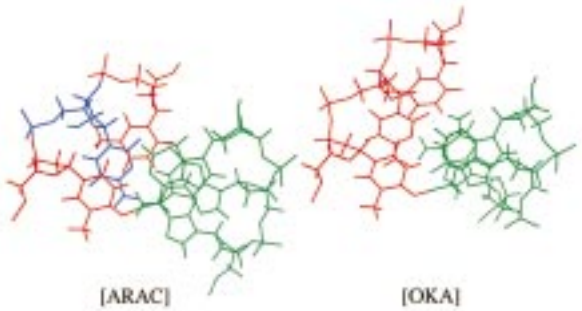

FIGURE 5: View along the dyad axis showing stacking between nucleosides in the DDR of the refined structure of [ARAC] (left) and the refined structure of [OKA] (right). For each duplex purines 4, 5, and 6 are shown in aqua and pyrimidines 19, 20, and 21 are shown in red, except for cytarabine in [ARAC] that is shown in blue. Examination of helical parameters (Supplementary Information) shows values similar to B-form values for helical parameters in [ARAC] and deviations from B-form helical parameters for [OKA]. This view along the dyad axis shows that adoption of non-B-form helical parameters by [OKA] in the DDR results in more efficient stacking between the adjacent purine residues in the DNA strand of [OKA] relative to [ARAC].

pucker. The NMR spectral data for the DDR of [OKA] also clearly indicate adoption of B-form geometry (Supplementary Information). The 100 ms mixing time NOESY spectrum for [OKA] shows relatively strong intraresidue H8/H6−H2′ and weak interesidue H8/H6−H2″ NOEs for the DDR. ECOSY data also indicate relatively greater $^3J_{1'-2'}$ (8−9 Hz) and lesser $^3J_{1'-2''}$ (6−8 Hz) scalar couplings, and the absence of observable $^3J_{3'-4'}$ and $^3J_{2''-3'}$ scalar couplings. Similar spectroscopic patterns were also observed for [ARAC]. Since the DDR of [ARAC] contains the site of cytarabine substitution, the two model Okazaki fragments may be expected to differ considerably in this region. In fact, the structures of the DDR for [ARAC] and [OKA] are very similar (rmsd ∼0.8 Å; Figure 2). As will be described in greater detail below, cytarabine substitution induces a bend into the duplex that affects the global morphology of the model Okazaki fragment resulting in a much poorer overall fit between [ARAC] and [OKA] (rmsd ∼4.1 Å) than is the case for the DDR alone.

Despite the near uniform adoption of sugar puckers characteristic of B-form geometry in the DDR of [OKA], backbone torsional angles and base parameters for this region show considerable variance from characteristic B-form values (Supplementary Information). In particular, maximization of base stacking by the five consecutive purines in the DDR causes these residues to adopt values for a number of helical parameters not characteristic of B-form DNA. Twist is relatively larger between G5 and A6 of [OKA], and relatively smaller between A4 and G5, compared to canonical B-form geometry (*51*). Roll is relatively larger between A3 and A4 compared to canonical B-form geometry. The net effect of these alterations in helical parameters for the purine-rich strand of the DDR from values characteristic of B-form geometry is more efficient stacking among adjacent purines. A comparison of purine stacking in the DDR for the refined structure of [OKA], and for [ARAC], is shown in Figure 5. A summary of the torsional and helical parameters for [OKA] and [ARAC] is included in the Supplementary Information.

Comparison of DDR structure for [ARAC] relative to [OKA] reveals that the DDR for both model Okazaki fragments are similar, although decreased base stacking is observed for adjacent purines in the DNA strand of [ARAC] (Figure 5). Analyses of the helical parameters and torsion angles for the DDR of [ARAC] reveals that the helical parameters for the DDR of [ARAC] are, in fact, consistently more similar to canonical B-form DNA than was the case for [OKA] (Supplementary Information). In particular, twist in [OKA] was relatively larger between G5 and A6 and relatively smaller between A4 and G5, compared to canonical B-form geometry (*51*). Roll was relatively larger in [OKA] between A3 and A4, compared to canonical B-form geometry. The net effect of these alterations in helical parameters for the purine-rich strand of the DDR of [OKA] was more efficient stacking among adjacent purines in the DNA strand (Figure 5). In contrast to what was observed for the DDR of [OKA], twist and roll parameters for [ARAC] fall within a narrower range that is similar to canonical B-form values, even for those base steps that involve the site of cytarabine substitution. The net effect of uniform adoption of these more B-form values for the helical parameters of [ARAC] relative to [OKA] is reduced base stacking among the adjacent purines in the DNA strand of [ARAC] (Figure 5).

The backbone parameters are altered at, and near, the site of arabinosyl substitution of [ARAC] relative to [OKA], resulting in an increased bend in the helical axis of [ARAC]. Specific alterations in [ARAC] that contribute to the increased bending are decreased values for delta and the amplitude of pucker for T19, the site adjacent to the cytarabine substitution, and increased values for zeta and the amplitude of pucker for aC20, the site of substitution (Supplementary Information). These residues also had the largest changes in chemical shift in [ARAC] relative to [OKA] (Table 3). Both H1′ and H2″ of T19 move significantly (∼0.15 ppm) downfield in [ARAC] relative to [OKA], consistent with an alteration in torsion angles and/or pucker amplitude for this nucleoside. Conversely H6, H5, and H1′ of aC20 move upfield a similar amount (∼0.15 ppm) in [ARAC] relative to [OKA]. The single largest change in chemical shift in [ARAC] relative to [OKA] occurs for H2″ of aC20 that moves 1.88 ppm downfield, relative to the corresponding value for C20 in [OKA]. While the magnitude of this change in chemical shift is largely due to the inductive electron withdrawing effect of the arabinosyl hydroxyl, a structural component likely contributes to the change in chemical shift, as well. The purines in the complementary strand across from the site of arabinosyl substitution show somewhat decreased values for the torsion angle alpha at A4, G5, and A6 and slight alterations in chemical shift for the base and sugar protons of these nucleosides (Supplementary Information). Decreased intensity is also observed for the H2 to H2 NOEs between A6 and A18, and A3 with both A2 and A4, in [ARAC] relative to [OKA]. The observed reduction in intensities for these NOEs is indicative of reduced base stacking in this region. Changes in chemical shift for [ARAC] compared to [OKA] are presented in Table 3. The $^3J_{1'-2''}$ scalar coupling for aC20 is readily apparent in a spectral region for which cross-peaks from both deoxyribo- and ribonucleotides are absent (Supplementary Information).

HDR Structures. The HDR of [OKA] consists of ribonucleosides g13−g16 and deoxyribonucleosides C9−C12 (Figure 1). Each of the RNA residues in the HDR adopts a C3′-endo sugar pucker, the conformation characteristic of

A-form double helices. The sugar pucker for DNA residues in the HDR depends on the position of the deoxyribonucleoside. C9 and C10 in the interior of [OKA] adopt time-averaged sugar puckers with *P* values near 100°, while T11 and C12 near the terminus adopt C2′-endo sugar puckers (*P* ∼ 160°) characteristic of B-form DNA. The position dependence of the sugar pucker for deoxyribonucleosides in the HDR probably results from conformational averaging. A time-averaged sugar pucker intermediate between C2′-endo and C3′-endo is favored for DNA residues base paired to RNA, while a C2′-endo geometry is favored by deoxyribonucleosides near the terminus that are more susceptible to base pair opening. The HDR of [ARAC] adopts sequence-specific geometry similar to that observed for [OKA]. The structures of the HDR for [OKA] and [ARAC] are shown in Figure 2.

The NMR spectral data for the deoxyribonucleosides in the HDR of both [OKA] and [ARAC] also clearly indicate adoption of sequence-specific conformations. The 100 ms mixing time NOESY spectra for [OKA] shows relatively strong intraresidue H8/H6−H2′ and weak interesidue H8/H6−H2″ NOEs for T11 and C12 in the HDR, while the inter- and intraresidue NOEs are similar for C9 and C10. A similar pattern is observed in the 150 ms mix time NOESY spectrum of [ARAC]. ECOSY data for both model Okazaki fragments also indicate relatively greater $^3J_{1'-2'}$ and lesser $^3J_{1'-2''}$ scalar couplings and the absence of observable $^3J_{3'-4'}$ and $^3J_{2''-3'}$ scalar couplings for T11 and C12. $^3J_{3'-4'}$ scalar couplings are evident for C9 and C10 of both model Okazaki fragments. The A-form geometry of the ribonucleosides is characterized by undetectable $^3J_{1'-2'}$ but readily measurable $^3J_{3'-4'}$ scalar couplings, under the experimental conditions used. RNA residues were also characterized by strong interesidue, and less intense intraresidue, H8−H2′ NOEs, consistent with adoption of C3′-endo sugar puckers.

JR Structures. The DDR and HDR of both [OKA] and [ARAC] intersect at the junction region (JR) that consists of two base pairs. The DNA strand in the JR consists of two pyrimidine residues (T7 and T8), while the hybrid strand consists of two purine nucleosides (a17 and A18). The sugar pucker of the sole ribonucleoside (a17) in the JR of [OKA] is C3′-endo. Interestingly, although the sugar puckers for all four nucleosides in the JR of [OKA] differ considerably from the C2′-endo sugar pucker characteristic of B-form helical geometry, the base pair overlap in this region closely resembles that which occurs in canonical B-form geometry (Figure 3). Extensive base−base overlap occurs between the adjacent purine nucleosides a17 and A18 of the hybrid strand, while minimal base−base overlap is observed between the complementary pyrimidines T7 and T8 of the DNA strand. Intrastrand P−P distances for both the hybrid and DNA strands of [OKA] are also more similar to canonical B-form geometry than A-form, despite the deviation from C2′-endo sugar pucker. Overall, the coordinates for the JR of [OKA] match well with canonical B-form geometry (rmsd ∼ 1.1 Å). Helical parameter values in the JR are mainly indistinguishable from the adjacent helical regions, with the exception that base pair tilt at the A6-T7 step is more negative than other base pair steps within [OKA]. The geometrical features of the JR present in [OKA] are conserved in [ARAC]. The sugar pucker of the sole ribonucleoside (a17) in the JR is C3′-endo. Base pair overlap in this region resembles that which occurs in canonical B-form geometry, although it is decreased slightly relative to [OKA] (Figure 3). Extensive base−base overlap occurs between the adjacent purine nucleosides a17 and A18 of the hybrid strand, while minimal base−base overlap is observed between the complementary pyrimidines T7 and T8 of the DNA strand.

Groove Dimensions. The groove structure for the DDR of [OKA] is similar to that characteristic of the B-form, although considerable variability exists in this region (*51*). Near the terminus of the DDR, the minor groove is somewhat shallower and broader than canonical B-form DNA. Nearer to the JR, the minor groove is somewhat constricted relative to B-form values. The major groove width and small axial displacements in the DDR are also similar to values characteristic of B-form geometry. The minor groove structure for the DDR of [ARAC] is similar to that characteristic of B-form geometry, and its dimensions are somewhat less variable than those observed for [OKA]. In particular, the minor groove width, which was markedly constricted at G5 and A6 of [OKA], is characterized by nearly prototypical B-DNA values for these base pairs in the DDR of [ARAC], the region that includes cytarabine. The major groove width and small axial displacements in the DDR of [ARAC] are also similar to values characteristic of B-form geometry, although the major groove is constricted relative to B-form values immediately adjacent to the JR.

The groove structure for the HDR of [OKA] differs considerably from the generally B-form values observed in the DDR of this structure. The minor groove is considerably broader and shallower in the HDR than in the DDR, and in this respect, the groove structure in the HDR resembles A-form helical geometry. The major groove width and small axial displacements for base pairs in the HDR differ considerably from canonical A-form helical values and more closely resemble B-form geometry. The groove structure for the HDR of [ARAC] is similar to that observed in the HDR of [OKA]. Groove width parameters change rapidly in the JR for both model Okazaki fragments with the minor groove being narrow and deep near the DDR, and wide and shallow near the HDR. The major groove is similar to B-DNA-like geometry, however, remaining broad and somewhat shallow. Axial displacements in the JR are small and resemble B-DNA values. Numerical values for the groove dimensions of [OKA] and [ARAC] are included in the Supplementary Information.

DISCUSSION

Determining the structures of Okazaki fragments is important for understanding the structural basis for DNA replication, and for the rational design of drugs that block replication (*1*, *2*, *52*). In the present study, we have determined the NMR solution structures of [OKA] and [ARAC], model Okazaki fragments with sequence derived from a frequent site for initiation of primase during lagging strand replication of the SV-40 viral genome (*19*, *20*). Overall, the solution structure of [OKA] resembles B-DNA, with an rmsd of 0.6 Å for residues in the DDR. Significant local structural variability occurs in all regions of the molecule, and these distinct structural features such as variability in minor groove dimensions and overall curvature

may be significant for the biological function of Okazaki fragments, as well as provide a structural basis for the design of antiproliferative agents (*53*). The structure of [ARAC] is similar to that of [OKA], and each structure may be considered in terms of three regions (DDR, HDR, and JR), with each region displaying characteristic morphology based on its unique nucleoside composition (Figure 1). The local structures for each of these regions in [ARAC] are similar to the same region in [OKA]. Nonetheless, the overall structure for [ARAC] shows a distinctly greater bend in the helical axis relative to [OKA], although only a few helical parameters are impacted by cytarabine substitution (Supplementary Information). The increased helical bend of [ARAC] relative to [OKA] may contribute to the propensity of cytarabine to inhibit chain elongation of the lagging strand during DNA replication and provide a structural basis for the anticancer activity of cytarabine (*21*, *22*).

Comparison of Okazaki Fragments. Previous studies investigating Okazaki fragment structure have resulted in different conclusions, even for the same sequence under different experimental conditions. X-ray analysis for the sequence r(gcg)d(TATACCC)−d(GGGTATACGC) indicated adoption of A-form geometry throughout this model Okazaki fragment, including the DDR of this structure (*29*). The authors concluded that adoption of C3′-endo geometry by the three RNA residues locked the entire decamer into the A-conformation. An NMR structure of this same duplex in solution indicated that this Okazaki fragment was neither A- nor B-form in its entirety (*30*). Rather, the structure adopted in solution was a chimeric mixture of hybrid form (H-form) and B-form structural morphologies. The DDR of this model Okazaki fragment had sugar conformations, intrastrand P−P distances, and minor groove dimensions typical of those found in B-form duplexes. The HDR of this model Okazaki fragment in solution had C3′-endo sugar puckers for the RNA residues and O4′-endo sugar puckers for the DNA residues. A structural discontinuity was observed between the DDR and HDR for this model Okazaki fragment in solution with a bend of 18° at the junction. A bend of similar magnitude (26°) in Okazaki fragments had been predicted from previous model building studies, while the solution structure of [OKA] in the present study indicates that a bend of 22° occurs for this sequence (*23*−*25*). Bending of chimeric hybrid duplexes has been proposed to provide a driving force for recognition by reverse transcriptase, and bending of Okazaki fragments may be significant in regulating replication of the lagging strand during DNA synthesis (*54*, *55*).

The model Okazaki fragment [OKA] considered in the present study differs considerably in sequence from the model Okazaki sequence investigated previously using X-ray crystallography and solution NMR spectroscopy (*29*, *30*). In particular [OKA] contains 12 rather than 10 base pairs, with the two additional base pairs adding to the HDR portion of the model Okazaki fragment. In this respect, [OKA] may provide a more reasonable model for Okazaki fragment structure in vivo since RNA primase generally incorporates more than three ribonucleotides prior to extension by DNA polymerase (*56*). Interestingly, the increased percentage of ribonucleotides in [OKA] and [ARAC] relative to the model Okazaki fragment studied in refs 29 and 30 does not cause the entire duplex to adopt A-form geometry in solution. Rather, the H-form morphology is extended in the HDR of [OKA] of [ARAC]. These results support the conclusion that the adoption of A-form geometry by Okazaki fragments in the crystalline state results from crystal packing forces, and that the solution structure of Okazaki fragments is polymorphic with different characteristic geometries occurring for the DDR, the HDR, and the JR.

Effect of Cytarabine. Only subtle changes to helical parameters are induced by cytarabine substitution. The moderate effect of cytarabine substitution to the structure of the model Okazaki fragment is reflected in the low rmsd between the DDR of [OKA] and [ARAC] (∼0.8 Å). These subtle alterations in helical parameters resulting from cytarabine substitution are structurally significant because they result in an increased bend angle between the two principal helical regions in the model Okazaki fragment (Figure 4). Thus, while either the DDR or HDR of [ARAC] may be superimposed upon the like region of [OKA] with relatively low rmsd (Figures 2), increased helical bend in [ARAC] resulting from cytarabine substitution causes the overall rmsd between [ARAC] and [OKA] to be greater than regional congruity would otherwise imply. Cytarabine thus induces a gross alteration to the morphology of the model Okazaki fragment through minor, selective alterations in helical parameters. This increased helical bend in Okazaki fragments substituted with cytarabine may interfere with the successful completion of replication through relative displacement of the site of extension from the origin of the Okazaki fragment. These sites may be relatively distal in primary sequence (∼100 nucleotides) but brought close together as a consequence of compaction or nucleosome formation (*57*).

Previous Cytarabine Studies. The importance of cytarabine for the treatment of leukemia has resulted in a number of investigations aimed at detecting structural alterations in nucleic acids substituted with cytarabine (*58*−*64*). Monomeric cytarabine adopts a C2′-endo sugar pucker in the crystalline state, the same sugar pucker adopted by aC20 of [ARAC] in the present investigation (*58*). The C2′-endo sugar pucker of cytarabine was stabilized by an intramolecular hydrogen bond to O5′ and, although such hydrogen bond formation cannot be detected directly by the usual solution NMR techniques, the final structure of [ARAC] includes a similar hydrogen bond (Figure 1). Other structural studies have also determined that cytarabine adopts a C2′-endo sugar pucker in a DNA duplex (*63*), although other studies have concluded that other sugar puckers occur for cytarabine-substituted DNA duplexes (*64*). A detailed solution NMR study of the Drew-Dickerson dodecamer sequence with and without cytarabine substitution provided the first high-resolution information about the effects of cytarabine on duplex DNA structure in solution (*64*). Cytarabine substitution did not produce a large change in the overall structure of this DNA duplex (rmsd ∼ 1.3 Å), and structural effects were limited to the site of cytarabine substitution and the adjacent residues. The observed subtle differences in helical parameters and torsion angles were interpreted as being due to potential steric interactions and hydrogen bond formation between O2′ and O2′H of the arabinosyl sugar and the base proton and phosphate backbone of the neighboring nucleoside.

The present study differs from previous investigations in focusing on the effects of cytarabine on the structure of a

model Okazaki fragment rather than a DNA duplex. Although cytarabine is a deoxycytidine analogue, its biological effects are mainly manifest at replication of the lagging strand during DNA synthesis, and it is in the context of Okazaki fragment structure that cytarabine inhibits the successful completion of DNA replication in malignant cells (*21*, *22*). In the present study, the effects of cytarabine substitution on the local structure of the DDR of [ARAC] are slight, with rmsd's of similar magnitude to those reported previously. However, the effect of cytarabine on the overall morphology of the model Okazaki fragment is significantly larger than that previously observed in DNA duplexes. This larger structural perturbation arises from the small changes in helical parameters and torsion angles caused by cytarabine substitution increasing the bend angle of the model Okazaki fragment. Studies of other model Okazaki fragment structures, both in solution and in the crystalline state, have indicated a bend in the helical axis between the DDR and HDR (*29*, *30*). In the case of the sequence investigated in the present study, cytarabine increases this bend angle. While the types of local structural alterations induced by cytarabine are likely to be similar in different systems, the overall effects on nucleic acid structure are likely to be system-dependent.

Conclusions. The solution structures for [OKA] and [ARAC], model Okazaki fragments with sequence derived from a frequent site for initiation of primase during lagging strand replication of the SV-40 viral genome, have been elucidated using NMR spectroscopy and rMD simulations. These structures each represent an additional contribution to the limited number of studies available on Okazaki fragment structure. Although [ARAC] differs from other model Okazaki fragments studied in the inclusion of a non-native nucleoside, cytarabine, in the sequence investigated, the overall structural features of both model Okazaki fragments are similar to each other, and to other model Okazaki fragments. In particular, variability in the dimensions of the minor groove from the narrow, deep region in the DDR to the wide, shallow region in the HDR occurs in other model Okazaki fragment solution structures (*29*). Bending of the helical axis between the DDR and HDR appears to generally occur for model Okazaki fragments both in solution and in the crystalline state (*29*, *30*). These general structural features of model Okazaki fragments in solution are likely responsible for RNase H1 and FEN1 recognition and cleavage in vivo (*65*). Cytarabine substitution in the model Okazaki fragment considered in the present study affected helical parameters and torsion angles near the substitution, resulting in an increased bend in the helical axis. These results suggest that, mechanistically, cytarabine exerts its cytotoxic effects by inducing a greater than normal bend in the growing Okazaki fragment, causing the sites of initiation and extension of the Okazaki fragment to be dislocated relative to one another. Such a dislocation could interfere either with nucleosome positioning or in some type of proofreading activity, causing DNA extension to be halted (*66*). Additional studies will be required to determine the functional consequences of the observed alterations in Okazaki fragment structure resulting from cytarabine substitution, and to utilize this mechanistic information to improve chemotherapeutic regimens (*67*).

ACKNOWLEDGMENT

Thanks to Mr. Jinqian Liu for the synthesis of cytarabine phosphoramidite and Dr. R. T. Pon for the synthesis and purification of oligonucleotides.

SUPPORTING INFORMATION AVAILABLE

2D NMR spectra used in making the assignments of [OKA] and [ARAC], a summary of the torsion angles and helical parameters for both model Okazaki fragments, a summary of the groove dimensions for both duplexes, rmsd values between intermediate and final structures, Rx values from CORMA analyses, and a summary of helical parameters for [OKA] and [ARAC] (26 pages). Ordering information is available on any current masthead page.

REFERENCES

1. Kelman, Z., Hurwitz, J., and O'Donnell, M. (1998) *Structure 6*, 121−125.
2. Dutta, A., and Bell, S. P. (1997) *Annu. Rev. Cell Dev. Biol. 13*, 293−332.
3. Toone, W. M., Aerne, B. L., Morgan, B. A., and Johnston, L. H. (1997) *Annu. Rev. Microbiol. 51*, 125−149.
4. Broach, J. R., Li, Y. Y., Feldman, J., Jayaram, M., Abraham, J., Nasmyth, K. A., and Hicks, J. B. (1983) *Cold Spring Harbor Symp. Quant. Biol. 2*, 1165−1173.
5. Foiani, M., Lucchini, G., and Plevani, P. (1997) *Trends Biochem. Sci. 22*, 424−427.
6. Tomkinson, A. E., and Mackey, Z. B. (1998) *Mutat. Res. 407*, 1−9.
7. Ogawa, T., and Okazaki, T. (1980) *Annu. Rev. Biochem. 49*, 421−457.
8. Gilboa, E., Mitra, S. W., Goff, S., and Baltimore, D. (1979) *Cell 18*, 93−100.
9. Bullock, P. A. (1997) *Crit. Rev. Biochem. Mol. Biol. 32*, 503−568.
10. Bentley, N. J., and Carr, A. M. (1997) *Biol. Chem. 378*, 1267−1274.
11. McIntosh, E. M., and Haynes, R. H. (1997) *Acta Biochim. Pol. 44*, 159−171.
12. Pratt, W. B., Ruddon, R. W., Ensminger, W. D., and Maybaum, J., Eds. (1994) *The Anticancer Drugs*, 2nd ed., Oxford Press, New York.
13. Caceres-Cortes, J., Sugiyami, H., Ikudome, K., Saito, I., and Wang, A. H.-J. (1997) *Eur. J. Biochem. 224*, 818−828.
14. Wu, W., Vanderwall, D. E., Lui, S. M., Tang, X., Turner, C. J., Kozarich, J. W., and Stubbe, J. (1996) *J. Am. Chem. Soc. 118*, 1268−1280.
15. Lown, J. W. (1993) *Pharmacol. Ther. 60*, 185−214.
16. Gmeiner, W. H. (1998) *Curr. Med. Chem. 5*, 115−135.
17. Higashigawa, M., Ido, M., Kuwabara, H., Hori, H., Ohkubo, T., Kawasaki, H., Sakurai, M., Taniguchi, K., and Hamazaki, M. (1991) *Leuk. Res. 15*, 255−262.
18. Johnston, P. G., Takimoto, C. H., Grem, J. L., Fidias, P., Grossbard, M. L., Chabner, B. A., Allegra, C. J., and Chu, E. (1997) Antimetabolites in *Cancer Chemotherapy and Biological Response Modifiers 17*, pp 1−39, Elsevier, Amsterdam.
19. Gmeiner, W. H., Skradis, A., Pon, R. T., and Liu, J−Q. (1998) *Nucleic Acids Res. 26*, 2359−2365.
20. Vishwanatha, J. K., Coughlin, S. A., Weselowski-Owen, M., and Baril, E. F. (1986) *J. Biol. Chem. 261*, 6619−6628.
21. Kufe, D. W., Munroe, D., Herrick, D., Egan, E., and Spriggs, D. (1984) *Mol. Pharmacol. 26*, 128−134.
22. Ross, D. D., Cuddy, D. P., Cohen, N., and Hensley, D. R. (1992) *Cancer Chemother. Pharmacol. 31*, 61−70.
23. Selsing, E., Wells, R. D., Early, T. A., and Kearns, D. R. (1978) *Nature 254*, 249−250.
24. Selsing, E., Wells, R. D., Alden, C. J., and Arnott, S. (1979) *J. Biol. Chem. 254*, 5417−5422.
25. Selsing, E., and Wells, R. D. (1979) *J. Biol. Chem. 254*, 5410−5416.

26. Wang, A. H.-J., Satoshi, F., van Boom, J. H., van der Marel, G. A., van Boekel, S. A. A., and Rich, A. (1982) *Nature 299*, 601−604.
27. Mellema, J.-R., Haasnoot, C. A. G., van der Marel, G. A., Wille, G., van Boekel, C. A. A., van Boom, J. H., and Altoona, C. (1983) *Nucleic Acids Res. 11*, 5717−5738.
28. Fujii, S., Matsui, S., Tomita, K., Orita, M., Tanaka, T., and Uesugi, S. (1989) *Nucleic Acids Symp. Ser. 21*, 67−68.
29. Egli, M., Usman, N., Zhang, S., and Rich, A. (1992) *Proc. Natl. Acad. Sci. U.S.A. 89*, 534−538.
30. Salazar, M., Federoff, O. Y., Zhu, L., and Reid, B. R. (1994) *J. Mol. Biol. 241*, 440−455.
31. Beardsley, G. P., Mikita, T., Klaus, M. M., and Nussbaum, A. L. (1988) *Nucleic Acids Res. 16*, 9165−9176.
32. States, D. J., Haberkorn, R. A., and Ruben, D. J. (1982) *J. Magn. Reson. 48*, 286−292.
33. Griesinger, C., Sorenson, O. W., and Ernst, R. R. (1985) *J. Am. Chem. Soc. 107*, 6394−6396.
34. Borgias, B. A., and James, T. L. (1990) *J. Magn. Reson. 87*, 475−487.
35. Carper, W. R., and Keller, C. E. (1997) *J. Phys. Chem. A 101*, 3246−3250.
36. Kim, S.-G., Lin, L.-J., and Reid, B. R. (1992) *Biochemistry 31*, 3564−3574.
37. Bax, A., and Lerner, L. (1988) *J. Magn. Reson. 79*, 429−438.
38. Haasnoot, C. A. G., de Leeuw, F. A. A. M., and Altona, C. (1980) *Tetrahedron 36*, 2783−2792.
39. Altona, C., and Sundaralingham, M. (1972) *J. Am. Chem. Soc. 94*, 8205−8212.
40. Singh, U. C., Weiner, S. J., and Kollman, P. (1985) *Proc. Natl. Acad. Sci. U.S.A. 82*, 755−759.
41. Sahasrabudhe, P. V., and Gmeiner, W. H. (1997) *Biochemistry 36*, 5981−5991.
42. Sahasrabudhe, P. V., Pon, R. T., and Gmeiner, W. H. (1996) *Biochemistry 35*, 13597−13608.
43. Baleja, J. D., Pon, R. T., and Sykes, B. D. (1990) *Biochemistry 29*, 4828−4839.
44. Mujeeb, A., Kerwin, S. M., Kenyon, G. L., and James, T. L. (1993) *Biochemistry 32*, 13419−13431.
45. Schmitz, U., Ulyanov, N. B., Kumar, A., and James, T. L. (1993) *J. Mol. Biol. 234*, 373−389.
46. Lavery, R., and Sklenar, H. (1990) CURVES 3.0. Helical Analysis of Irregular Nucleic Acids, Laboratory of Theoretical Biology, CNRS, Paris.
47. Ravishanker, G., Swaminathan, S., Beveridge, D. L., Lavery, R., and Sklenar, H. (1989) *J. Biomol. Struct. Dyn. 6*, 669−699.
48. Borgias, B. A., and James, T. L. (1988) *J. Magn. Reson. 79*, 493−512.
49. Hare, D. R., Wemmer, D. E., Chou, S. H., Drobny, G., and Reid, B. R. (1983) *J. Mol. Biol. 171*, 319−336.
50. Arnott, S., and Hukins, D. W. L. (1972) *Biochem. Biophys. Res. Commun. 47*, 1504−1510.
51. Saenger, W. (1984) *Principles of Nucleic Acid Structure*, Springer, New York.
52. Sun, W., and Godson, G. N. (1998) *J. Mol. Biol. 276*, 689−703.
53. White, S., Szewczyk, J. W., Turner, J. M., Baird, E. E., and Dervan, P. B. (1998) *Nature 391*, 468−471.
54. Jacobo-Molina, A., Ding, J., Nanni, R. G., Clark, A. D., Jr., Lu, X., Tantillo, C., Williams, R. L., Kamer, G., Ferris, A. L., Clark, P., Hizi, A., Hughes, S. H., and Arnold, E. (1993) *Proc. Natl. Acad. Sci. U.S.A. 90*, 6320−6324.
55. Federoff, O. Y., Salazar, M., and Reid, B. R. (1993) *J. Mol. Biol. 233*, 509−523.
56. Sun, W., and Godson, G. N. (1998) *J. Mol. Biol. 276*, 689−703.
57. Luger, K., and Richmond, T. J. (1998) *Curr. Opin. Struct. Biol. 8*, 33−40.
58. Chwang, A. K., and Sundaralingham, M. (1973) *Nature 243*, 78−79.
59. Remin, M., Darzynkiewicz, E., Ekiel, I., and Shugar, D. (1976) *Biochim. Biophys. Acta 435*, 405−416.
60. Teng, M.-K., Liaw, Y.-C., van der Marel, G. A., van Boom, J. H., and Wang, A. H.-J. (1989) *Biochemistry 28*, 4923−4928.
61. Gao, Y.-G., van der Marel, G. A., van Boom, J. H., and Wang, A. H.-J. (1991) *Biochemistry 30*, 9922−9931.
62. Pieters, J. M. L., de Vroom, E., van der Marel, G. A., van Boom, J. H., and Altona, C. (1989) *Eur. J. Biochem. 184*, 415−425.
63. Pieters, J. M. L., de Vroom, E., van der Marel, G. A., van Boom, J. H., Koning, T. M. G., Kaptein, R., and Altona, C. (1990) *Biochemistry 29*, 788−799.
64. Schweitzer, B. I., Mikita, T., Kellogg, G. W., Gardner, K. H., and Beardsley, G. P. (1994) *Biochemistry 33*, 11460−11475.
65. Murante, R. S., Henricksen, L. A., and Bambara, R. A. (1998) *Proc. Natl. Acad. Sci. U.S.A. 95*, 2244−2249.
66. Ito, T., Tyler, J. K., and Kadonaga, J. T. (1997) *Genes Cells 2*, 593−600.
67. Hardman, J. G., and Limbird, L. E. (1996) Goodman & Gilman's *The Pharmacological Basis of Therapeutics*, 9th ed. McGraw-Hill, New York.

BI981702S